Applied Geochemistry 100 (2019) 293–304

Contents lists available at ScienceDirect

Applied Geochemistry

journal homepage: www.elsevier.com/locate/apgeochem

Geochemical conceptual model of BTEX biodegradation in an iron-rich aquifer

Elias Hideo Teramoto[a], Hung Kiang Chang[b,*]

[a] Laboratório de Estudos de Bacias and Centro de Estudos Ambientais, UNESP, Universidade Estadual Paulista, Av. 24A, 1515, Rio Claro, Sao Paulo, Brazil
[b] Departamento de Geologia Aplicada and Centro de Estudos Ambientais, UNESP, Universidade Estadual Paulista, Av. 24A, 1515, Rio Claro, Sao Paulo, Brazil

ARTICLE INFO

Editorial handling by Dr K Hanna

Keywords:
PCO_2
Lateritic aquifer
Reactive transport model
Iron reduction
Methanogenesis
Geochemical zoning

ABSTRACT

A geochemical conceptual model was developed to interpret long-term field monitoring data of the chemical speciation related to BTEX biodegradation in a tropical iron-rich aquifer that was contaminated by a large volume of jet fuel. Biodegradation under dissimilatory iron reduction is widely favored due to the abundance of iron oxides in the sediment. Concomitantly with iron-reduction, the methanogenesis pathway plays an important role in the microbial degradation of BTEX. The conceptual model was proposed to link the geochemical zonation with BTEX mineralization and secondary reactions. The representativeness of the chemical speciation of the studied hydrocarbon-contaminated aquifer is best supported when PCO_2 is fixed and dissolved oxygen, potentially present due to mass transfer from entrapped air, is considered in the model. These findings emphasize the need of both constraints to properly interpret BTEX biodegradation in a tropical iron-rich aquifer.

1. Introduction

Entrapped light nonaqueous phase liquid (LNAPL) in the saturated pores of an aquifer releases soluble compounds, such as BTEX (benzene, toluene, ethylbenzene and xylenes), into the water in response to mass transfer mechanisms (Miller et al., 1990). Decades of laboratory and field studies have provided solid evidence that indigenous microbial activity accounts for the metabolization of solubilized hydrocarbons under both aerobic and anaerobic conditions (Wiedemeier et al., 1999; National Council, 2000; Declercq et al., 2012). In the case where a sufficient supply of electron acceptors is available, biodegradation of solubilized hydrocarbons may occur quickly (Wiedemeier et al., 1999; National Council, 2000; Declercq et al., 2012). In several environments, due to an abundance of iron oxides in the sediment and limited availability of other electron acceptors, dissimilatory iron reduction is the prevailing mechanism of hydrocarbon metabolization.

Prior to the late 1980s, it was believed that hydrocarbon oxidation through the reduction of Fe(III) represented an abiotic reaction. The work by Lovley et al. (1989) was the first study to demonstrate that hydrocarbon oxidation under iron reduction is a microbial-mediated reaction. Since then, numerous studies have been developed to account for and to improve the understanding of hydrocarbon biodegradation under Fe(III) reduction. While some research has focused on the geochemical features of biodegradation under iron reduction (Baedecker et al., 1993; Rooney-Varga et al., 1999; Vencelides et al., 2007, Ng et al., 2014), other studies have focused on microbiological mediation (Bekins et al., 2001; Reguera et al., 2005; Weber et al., 2006; Klueglein et al., 2013; Esther et al., 2015). In tropical zones where warm and humid conditions prevail, the pedogenic process may promote the accumulation of ferruginous cementation or concretion (Tardy and Nahon, 1985; Schwertmann, 1988; Beauvais, 1999). This ferruginous horizon, known as laterite, is composed primarily of goethite (Tardy and Nahon, 1985). Due to their abundance, laterites represent an important and large source of electron acceptors to hydrocarbon oxidation in tropical zones.

Conceptual models of biogeochemistry of LNAPL contaminated sites encompass a complex overlap of several biogeochemical processes related to BTEX mineralization. Conceptually, the BTEX cleave is coupled with hydrocarbon breakdown reactions, including equilibrium states and the chemical reactions of inorganic by-products in pore water (Hunter et al., 1998; Mayer et al., 2002). Different conceptual models with particular features and geochemical constraints have been proposed to reproduce BTEX mineralization under iron reduction in field conditions, including Prommer et al. (2002), Schreiber et al. (2004), Vencelides et al. (2007), Miles et al. (2008), Colombani et al. (2009), and Ng et al. (2014). These works have all overlooked BTEX degradation under tropical environment.

The study site was contaminated by a large volume of jet fuel

* Corresponding author.
E-mail address: chang@rc.unesp.br (H.K. Chang).

https://doi.org/10.1016/j.apgeochem.2018.11.019
Received 1 March 2018; Received in revised form 20 November 2018; Accepted 20 November 2018
Available online 30 November 2018
0883-2927/

(Teramoto and Chang, 2017). The main mechanism of BTEX destruction is iron reduction. Hence, iron oxide present in the aquifer is expected to be reduced and solubilized. The available information suggests that the role of the combination of the two pronounced geochemical constraints in tropical environments is not generally reproduced in the reactive transport models related to BTEX biodegradation under dissimilatory iron reduction in the reviewed works. The first geochemical constraint is the oxidation of the reduced species, such as Fe^{2+} and CH_4, accounting for the redox state of the contaminated aquifer. The second constraint is related to the high partial pressure of CO_2 (PCO_2) that governs the equilibrium of the carbonated species in the groundwater.

Since air is the nonwetting phase in the multiphase context, a rising water table causes air entrapment when water invades the pores. This process of air entrapment was described by several authors, including Faybishenko (1995), Fry et al. (1997), Williams and Oostrom (2000), Holocher et al. (2003), Amos and Mayer (2006), Haberer et al., (2012), Marinas et al. (2013) and McLeod et al. (2015). According to Faybishenko (1995) the air entrapment occurs in the uppermost portion of the saturated zone creating a "quasi-saturated" zone in which large proportion of pore space is filled with entrapped air. Marinas et al. (2013) reported values of 54.5% of pore space occupied by entrapped air in their experiment, suggesting that large amount of oxygen may be potentially released. The effect of oxygen diffusion into groundwater, which occurs at the air/water interface, is well-recognized (Amos and Mayer, 2006; Haberer et al., 2012, 2015b). Oxygen can diffuse from entrapped air into groundwater over a potential timescale of years or decades (McLeod et al., 2015). Due to the presence of dissolved oxygen, the oxidation of the reduced by-products (e.g., Fe^{2+} and CH_4) can play a key role in the redox conditions of contaminated aquifers (Heron et al., 1994; Hunter et al., 1998; Mayer et al., 2002; Amos and Mayer, 2006). Despite its importance, few works (e.g., Vencelides et al., 2007, Miles et al., 2008) have included Fe^{2+} oxidation in reactive transport models for environments where BTEX biodegradation occurs and is mediated by iron reduction.

In contrast with by-product oxidation, the influence of natural PCO_2 is normally underestimated in the chemical speciation of hydrocarbon-contaminated aquifers, despite the ubiquitous role of PCO_2 in buffering the groundwater pH and governing the chemical equilibrium of the dissolved carbonate species (Clark and Fritz, 1997; Appelo and Pstma, 2005; Macpherson, 2009). High concentrations of CO_2 in soil and groundwater are usually associated with microbial-mediated hydrocarbon mineralization (Hinchee and Ong, 1992; Borden et al., 1995; Baker et al., 2000; Mayer et al., 2002; Fallgren et al., 2010; Sihota and Mayer, 2012; Mortazavi et al., 2013). Furthermore, the PCO_2 of shallow aquifers in both the saturated and the unsaturated zones may be 1 to 2 orders of magnitude larger when compared to the atmosphere under natural conditions (Brook et al., 1983; Appelo and Pstma, 2005; Clark and Fritz, 1997; Lee, 1997; Kessler and Harvey, 2001; Macpherson, 2009; Bordignon et al., 2015). PCO_2 is particularly elevated in tropical environments (Brook et al., 1983; Kessler and Harvey, 2001) where the soil respiration rate is high. By presuming its importance, the evaluation of the biodegradation of organic contaminants employed in the reactive transport models requires embracing the high natural PCO_2 levels to improve the reliability of the conceptual models related to BTEX biodegradation.

The present study presents a geochemical conceptual model of BTEX biodegradation based on the long-term monitoring of BTEX concentration and geochemical parameters in a lateritic aquifer that was contaminated by a large volume of jet fuel. Most geochemical studies related to hydrocarbon mineralization were carried out in Europe and North America, where the temperate climate dominates. Thus, to best interpret the monitored geochemical data collected at the study site, a conceptual model encompassing specific features of tropical climates is proposed.

2. Site description

The study site is in the municipality of Paulínia, São Paulo, Brazil. A large volume of jet fuel is present in the subsurface, with an estimated volume of 520 m^3 (Pede, 2009). The contamination was identified during a site investigation in 2002, and an active remediation based on the pump-and-treat technique has been operating since 2005. Initially, the remediation was operated with four pumping wells. From 2008 to 2009, five additional wells were incorporated into the system. From 2010 to 2011, the remediation was paused, and from 2011 to present, the operation has resumed with 20 active pumping wells (Teramoto and Chang, 2017). The extracted fluids were separated in the oil-water separation tanks. While the oil is stored in the waste tanks, the water is sent to the effluent treatment plant to remove the organic compounds and later discarded into the river.

To determine the limit of the LNAPL spread and the plumes of the dissolved phase of BTEX compounds, 117 monitoring wells were installed in an area of 264,600 m^2. Most of the monitoring wells are 14 m deep with a 4- to 5-m screen section and have been installed to leave at least 2 m of the screen section above the water table to prevent the top of the screen section from falling below the water table during periods with a high water table. The monitoring wells referred to as deep are 15–18 m in depth and short-screened (1 m). The deep monitoring wells were installed next to regular monitoring wells to determine the vertical distribution of the dissolved BTEX plume.

Fig. 1 shows the potentiometric map, the limit of the source zone, and the location of the monitoring and pumping wells in the study area. The source zone occupied an area of approximately 80,000 m^2.

2.1. Hydrogeological setting

The studied Cenozoic shallow aquifer is heterogeneous and is composed of clayey sands interfingered with coarse sand lenses, sandy clays and clayey silts (Bordignon et al., 2015). The geometry of the well-developed channel and the floodplain facies indicates a depositional environment dominated by meandering rivers. The hydraulic conductivities, as determined by slug tests performed on 64 monitoring wells, vary from 1.2×10^{-7} m/s to 2.4×10^{-4} m/s, with a geometric mean of 2.8×10^{-5} m/s (Teramoto and Chang, 2017). The average hydraulic gradient is 0.0036 in the northeastern region, and it increases to the southwest towards the discharge zone, reaching values of 0.0176.

3. Methodology

3.1. Geochemical characterization

Since May 2006, sampling campaigns have been carried out to evaluate the water quality of the groundwater, resulting in a long-term series of monitoring data. The samples were analyzed for volatile organic compounds (VOC) by gas chromatographic analysis and mass spectrometry (GC/MS), in accordance with USEPA method SW 8260C. The physical-chemical parameters were measured in situ using a multiparameter probe coupled with a low-flow water sampling unit. Alkalinity was measured by potentiometric titration by using a continuous addition of HCl, following USEPA method 310.1. Fe(II) was determined in the field immediately after sampling using a spectrophotometer with a 1,10-phenanthroline indicator. The geochemical simulations in the present study used the chemical analyses of the May 2012 sampling campaign (Table S1, Supplementary Material). This sampling campaign represents the most comprehensive campaign in terms of the number of sampled wells (69) and analyzed parameters.

Mineralogical characterization of the studied aquifer was conducted using core samples that were collected by a direct-push methodology. The aquifer mineralogy was identified using X-ray powder diffraction (Siemens 5000) and a scanning electron microscope (SEM) coupled to an energy dispersive analyzer (EDA) (Jeol JSM-6010 LA).

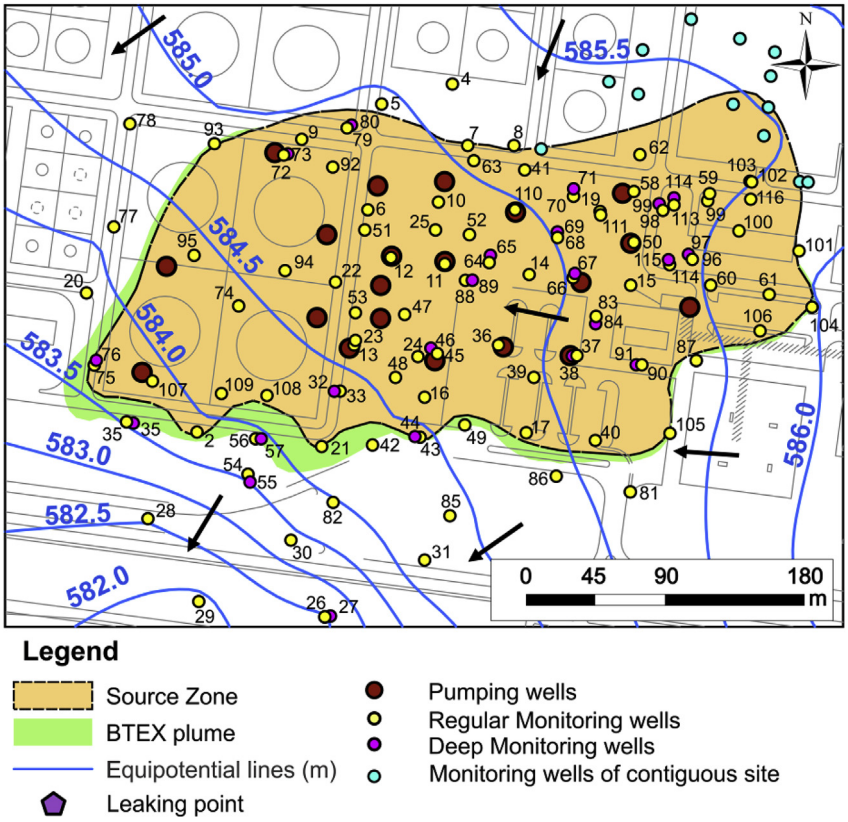

Fig. 1. Location of the monitoring and pumping wells in the study area and the delineation of the source zone contaminated by LNAPL (Teramoto and Chang, 2017).

3.2. Conceptual model formulation and validation

Based on the analytical results of the water quality monitoring and the chemical reactions associated with hydrocarbon biodegradation in the lateritic aquifer, a conceptual model was formulated to explain the chemical zonation affecting the contaminated groundwater.

4. Results

4.1. Geochemistry

The mineral phases that were identified in the studied aquifer were quartz (SiO_2), kaolinite ($Al_2Si_2O_5(OH)_4$), muscovite ($KAl_2(AlSi_3O_{10})(OH)_2$) and goethite (FeO(OH)) (Fig. 2), compatible with the lateritic nature of the studied aquifer. The X-ray diffraction of core samples reveals that goethite is abundant in the pristine sample (Fig. 2a) and absent in the core samples collected in the center of the source zone (Fig. 2b).

Due to an iron abundance in the aquifer (Fig. 3a), biodegradation by iron reduction was an important mechanism for BTEX mineralization. The biodegradation of the BTEX compounds, as represented by toluene, occurred under the reductive goethite solubilization. Fig. 4a shows a typical SEM image of the samples collected in the saturated zone of the uncontaminated aquifer (Well 20 at 11.8 m depth), in which it is possible to recognize the abundance of goethite microcrystals coating the sand grains. In contrast, the contaminated areas show a very low amount of iron oxides or even complete depletion (Fig. 4b) due to the active biodegradation (Well 45 at 12.5 m depth).

The high aqueous concentration of Fe^{2+} in the source zone and the abundance of iron oxides in the aquifer suggest that iron reduction is the primary reaction related to the microbial-mediated hydrocarbon degradation. Based on the available information, Fig. 4a–c presents the distribution of the dissolved Fe^{2+}; higher concentrations are observed within the source zone limits, and lower concentrations are observed outside of the source zone due to the continuous oxidation.

The monitoring wells reveal the Fe2+ concentration presents a large variation over time, inversely related to the water table fluctuation (Fig. 5a–d).

Fig. 6 illustrates the distribution of the CH_4 measured in the field. Similar to aqueous Fe^{2+}, a higher dissolved CH_4 concentration is found within the source zone limits, whereas a lower CH_4 concentration occurs outside the source zone due to the increased aquifer oxygenation.

Similar to Fe^{2+}, the CH_4 concentration presents a large variation over time, inversely related to the water table fluctuation (Fig. 7a–d).

4.2. Geochemical conceptual model

Based on the large data set collected during the successive investigations and monitoring of water quality, a conceptual model is proposed to encompass the effect of specific features related to subtropical and tropical environments on the chemical speciation of hydrocarbon mineralization. The major chemical and physical processes controlling the BTEX biodegradation and associated reactions are described below.

The study site is located in a tropical climate zone and encompasses specific conditions that are infrequently observed in temperate climate zones, where most of the earlier studies have been conducted. However, these conditions are crucial for accurately assessing hydrocarbon-contaminated aquifers. For example, the groundwater temperatures are typically above 26 °C throughout the year, so the microbial assimilation of hydrocarbons in the subsurface is broadly favored. Due to an accumulated annual rainfall in excess of 1300 mm/year, the volume of groundwater recharge is high, which induced a wide range of water table fluctuations and produced conditions conducive to LNAPL entrapment. Since the LNAPL is typically entrapped, the volatilization of the volatile compounds is restricted, and the mass-transfer to

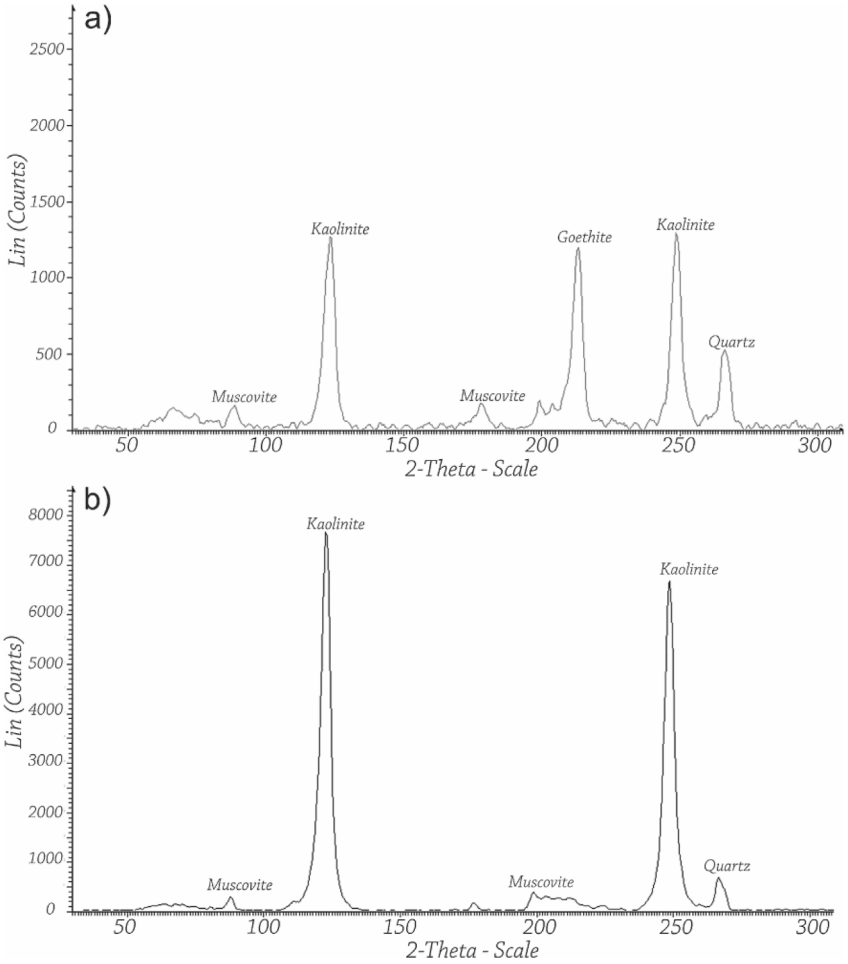

Fig. 2. X-ray diffractogram showing a) a pristine aquifer sample showing microcrystalline goethite crusts that coat the sand grains (Well 20 at 11.8 m depth) and b) a Fe^{3+}-depleted aquifer sample within the source zone (Well 45 at 12.5 m depth).

groundwater represented the primary mechanism for LNAPL source zone depletion. Additionally, the water table fluctuations created an important zone of entrapped air that greatly influence the redox conditions in the hydrocarbon-contaminated aquifers.

4.2.1. NAPL/water mass transfer

The wide range of the water table fluctuation creates a permanent entrapment of LNAPL in the saturated pores (Teramoto and Chang, 2017). Due to entrapment conditions, the most important mechanism operating in the BTEX depletion of LNAPL is represented by mass transfer to groundwater. LNAPL dissolution occurs when clean groundwater flushes the pores of the source zone. The movement of soluble compounds from the entrapped LNAPL to the clean water is a rate-limited (nonequilibrium) mass transfer phenomenon and can be calculated by multiplying the concentration driving force by the mass transfer coefficient and the specific interface area between the phases (Miller et al., 1990):

$$J = \frac{dC_a}{dt} = k_a a_{nw}(C_s - C), \quad (1)$$

Where J = the flow of mass from residual hydrocarbons to water ($ML^{-2}T^{-1}$), k_a = the coefficient of mass transfer (LT^{-1}), C_s = the maximum aqueous concentration of a soluble compound (ML^{-3}), C = the aqueous concentration of a soluble compound (ML^{-3}) and a_{nw} = the area of the specific interface between the water and NAPL (L^2).

Teramoto and Chang (2017) have shown that LNAPL saturation is higher in the center of the source zone and that LNAPL saturation decreases towards the edges. Since the LNAPL depletion with respect to BTEX compounds is related to the LNAPL saturation, the highest concentration of both the molar fraction of BTEX in the LNAPL and the effective solubility of BTEX in the groundwater are observed in the central portion of the source zone. Due to the variability in the effective solubility, the aqueous BTEX encompasses a wide range of concentrations (0.023 and 5.34 mg/L).

4.2.2. BTEX mineralization

Due to the iron abundance in the aquifer (Figs. 3a and 4a), typical of lateritic aquifers in tropical environments, biodegradation via iron reduction is an important mechanism for BTEX mineralization. The biodegradation of the BTEX compounds, represented by toluene, occurs under reductive goethite solubilization (Baedecker et al., 1993), per Eq. (2).

$$C_7H_8 + 36FeOOH + 65H^+ \rightarrow 51H_2O + 7HCO_3^- + 36Fe^{2+} \quad (2)$$

Several studies, such as Chapelle and Lovley (1992), Cozzarelli et al. (2001), Schreiber et al. (2004) and Miles et al. (2008), have demonstrated that biodegradation under Fe(III) reduction and methanogenesis usually occur concurrently. Eq. (3) describes the biodegradation of toluene by methanogenesis.

$$C_7H_8 + 5H_2O \rightarrow 4.5CH_4 + 2.5CO_2 \quad (3)$$

Figs. 4 and 6 reveal that the Fe^{2+} and CH_4 concentrations are high in the source zone, supporting the hypothesis that both pathways, BTEX biodegradation under iron reduction and methanogenesis, occur in the source zone.

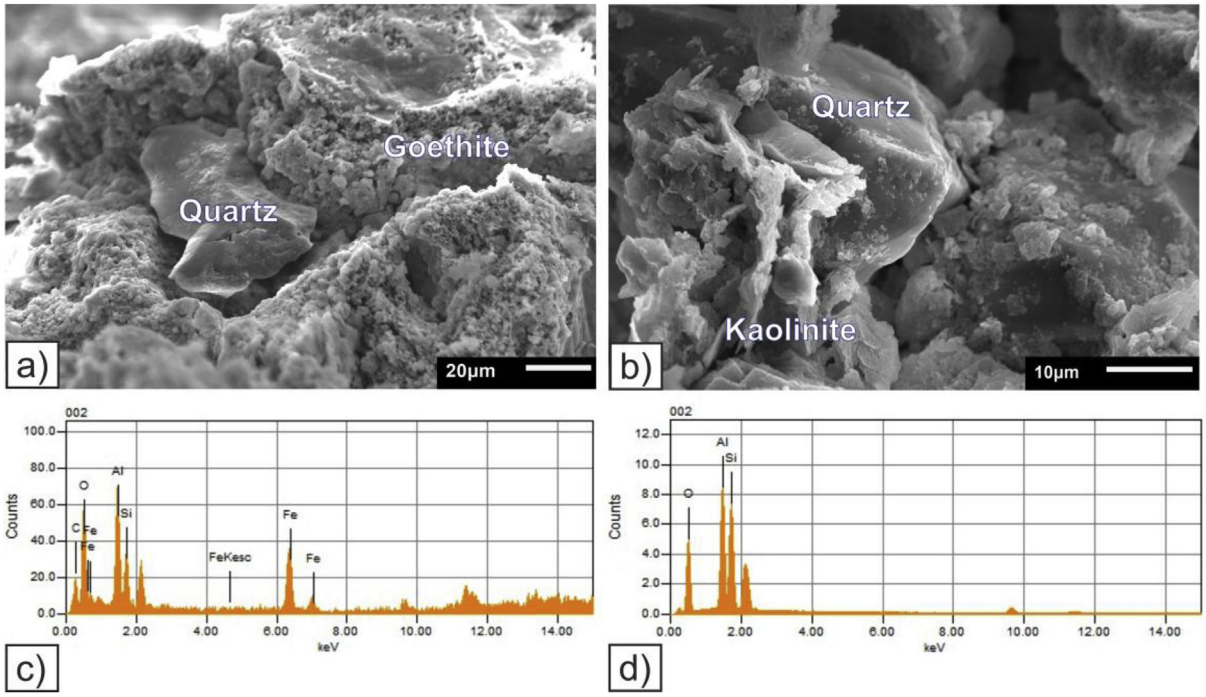

Fig. 3. SEM images: a) pristine aquifer sample showing microcrystalline goethite crusts that coat the sand grains (Well 20 at 11.8 m depth); b) Fe^{3+}-depleted aquifer sample due to goethite solubilization within the source zone (Well 45 at 12.5 m depth); c) EDS microanalysis of the pristine aquifer shown in Fig. 3a; d) EDS) microanalysis of the Fe^{3+}-depleted aquifer sample shown in Fig. 3b.

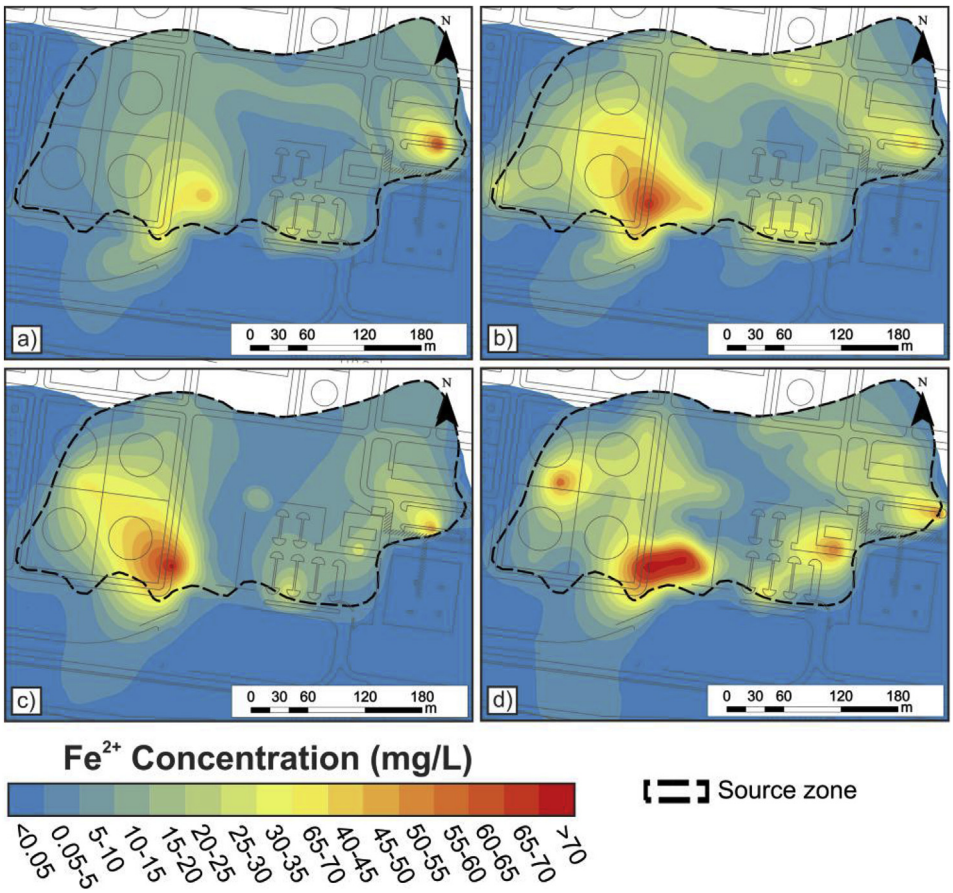

Fig. 4. Distribution of the Fe(II) concentration for the four sampling campaigns. a) June 2008; b) March 2010; c) March 2011; and d) May 2012. Higher values are observed within the source zone limits, and lower concentrations are observed outside of the source zone.

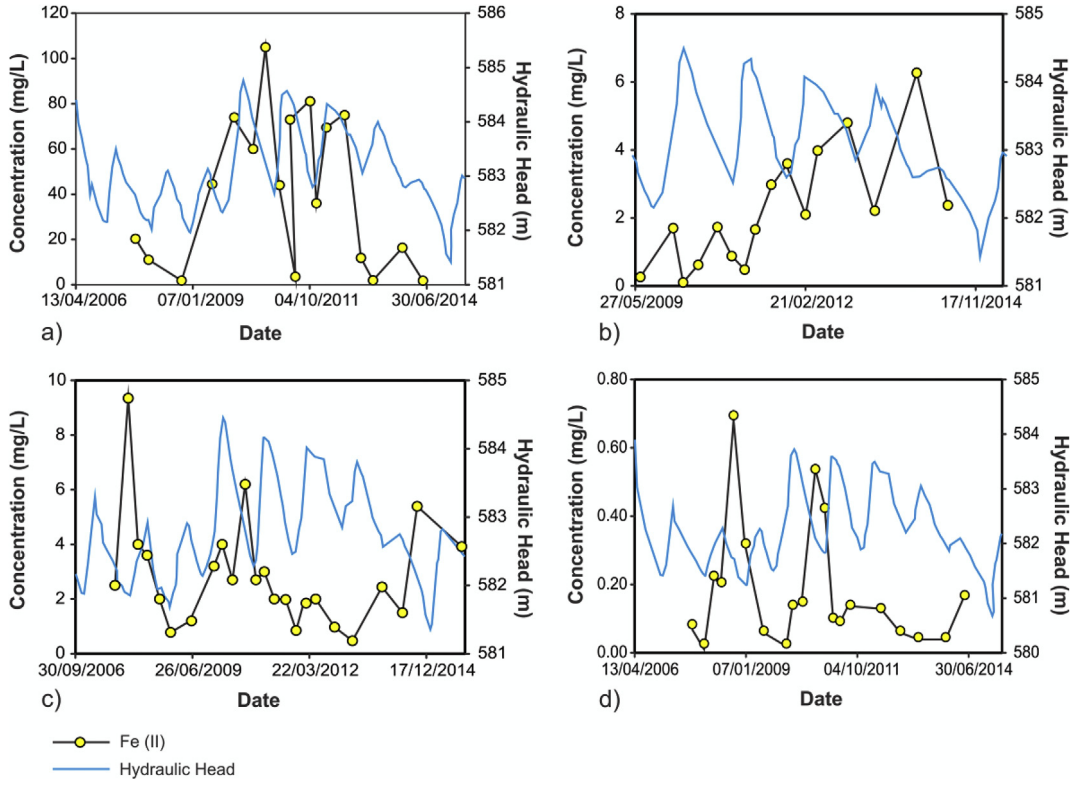

Fig. 5. Comparison of water table fluctuation and Fe(II) concentration variation over time. The sample locations are as follows: a) Well 32, center of the source zone; b) Well 81, downstream of the source zone; c) Well 67, downstream of the source zone; d) Well 30, downstream of the source zone.

4.2.3. Aquifer oxygenation

During groundwater recharge, water invades the pores, and air is partially trapped by capillary forces, similar to LNAPL. The mechanism of air entrapment is a well-known phenomenon that has been experimentally described by Faybishenko (1995), Fry et al. (1997), Williams and Oostrom (2000), Holocher et al. (2003), Amos and Mayer (2006), Haberer et al. (2012), Marinas et al. (2013) and McLeod et al. (2015). The uppermost portion of the saturated zone contains a variable proportion of entrapped air and represents the quasi-saturated zone (Faybishenko, 1995). The rate of the interphase transfer of oxygen (R_{oxygen}) from entrapped bubbles of air to the groundwater in the quasi-saturated zone is a function of both the concentration driving force and the air/water interfacial area, which may be represented by Eq. (4) (Geistlinger et al., 2005):

$$R_{oxygen} = \left(\frac{1}{r_b} - \frac{1}{\delta}\right)\cdot\left(\frac{A_g}{V}\right) * \left(a_w - \frac{a_g}{H}\right) \quad (4)$$

where r_b is the radius of the air bubble (m), δ is the stagnant film thickness (m), a_w is the activity of oxygen in the water (mol/L), a_g is the activity of oxygen in gas phase (mol/L), V is the volume of the air bubble (m^3), A_g is the surficial area of the entrapped air bubble, and H is the dimensionless Henry coefficient.

The mass transfer between entrapped air and groundwater (Eq. (4)) provides oxygen to the water, promoting oxidation of the by-products. In the source zone, it is probable that the oxygen released from the entrapped air rapidly oxidizes the aqueous Fe^{2+} (e.g., Haberer et al., 2015b) by microbial activity, maintaining the high concentration driving force. The oxidation of Fe^{2+} results in the unstable Fe $(OH)_3$ phase formation (Eq. (5)).

$$Fe^{2+} + 0.25O_2 + HCO_3^- + 0.5H_2O \rightarrow Fe(OH)_3 + 2CO_{2(aq)} \quad (5)$$

Fe(II) oxidation (Eq. (6)) is a pH-dependent reaction, and according to thermodynamic principles (Martin, 2005; Morgan and Lahav, 2007) and laboratory studies (Haberer et al., 2015a), at a pH value below 6, abiotic oxidation does not occur at high rates. However, Geroni & Sapsford (2011) have demonstrated that the values of Fe(II) oxidation rates measured in the field are 1–3 orders of magnitude higher than previously reported for laboratory studies at a similar pH range. Most likely, the higher rates in the field are related to catalysis mediated by autotrophic microbial activity of specific strains (e.g., *Gallionella ferruginea* and *Leptothrix ochracea*), since the biotic Fe(II) oxidation is several orders of magnitude greater than the abiotic Fe(II) oxidation (Katsoyiannis and Zouboulis, 2004). Most likely, the elevated kinetics of iron oxidation in the study field are related to microbial catalysis. According to several studies, including Breed et al. (1999), Vollrath et al. (2013) and Shirokova et al. (2016), biotic Fe(II) oxidation is a temperature-dependent reaction. The reaction rate of microbial-mediated oxidation increases with temperature until reaching an optimal temperature, after which the rate decreases. Since most of the optimal temperatures reported in the literature fall between 20 and 25 °C (e.g., Hallbeck et al., 1993; Yurt et al., 2002; El Gheriany et al., 2009), and the recorded temperature of groundwater in the study site is close to 26 °C, biotic Fe(II) oxidation should prevail. In our conceptual model, the released oxygen entrapped air promotes partial regeneration of the solubilized goethite within the source zone.

The mechanism to Fe(II) depletion accompanied by a pH decrease may be related to cationic exchange between Fe(II) and H^+ on the goethite surface (Ng et al., 2014). Since Dixit and Hering (2006) experiments have demonstrated that Fe^{2+} sorption on the goethite surface in an aqueous solution with pH varying between 4 and 6 (the range of pH measured in our study site) is very limited, we do not use this mechanism in our conceptual model.

Similar to Fe^{2+}, CH_4 is also oxidized (Eq. (6)) by catalysis by indigenous microbes that employ the diffused oxygen from entrapped air. Several methanotrophic strains, such as species from the genera Methylomonas, Methylocaldum, and Methylobacter (Newby et al., 2004; McDonald et al., 2006), are capable of oxidizing the dissolved methane, producing the enzyme methane monooxygenase to cleave the C—H

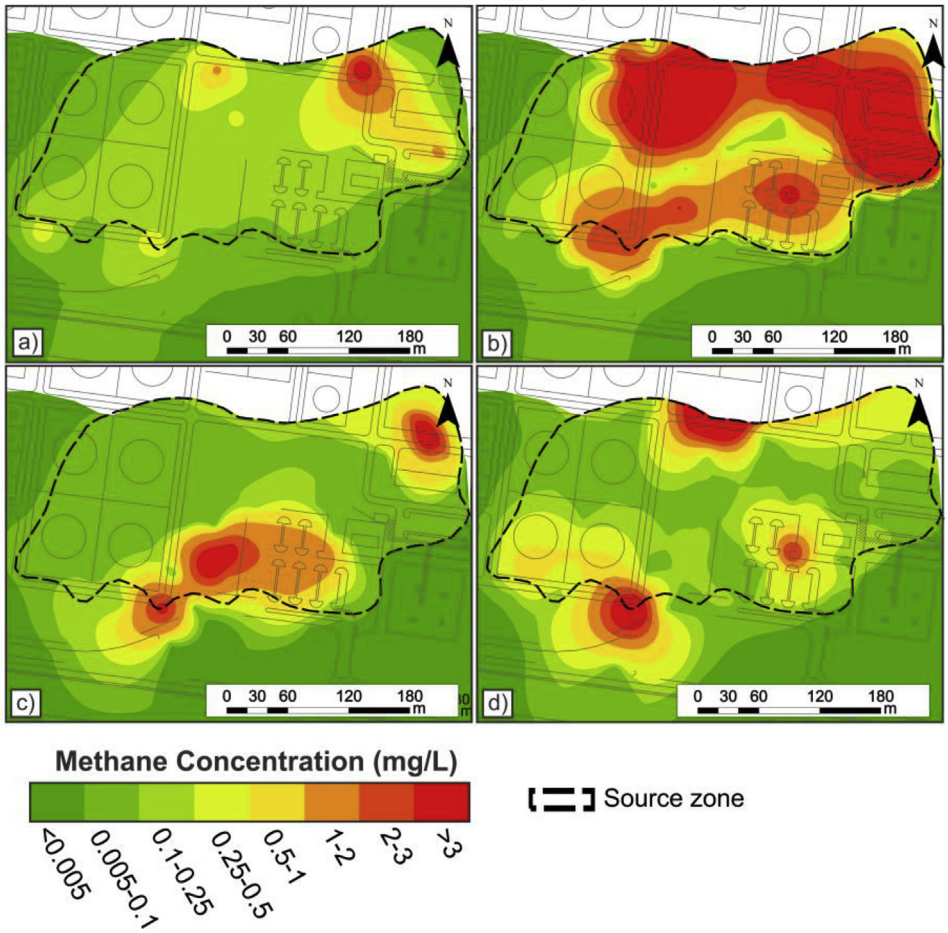

Fig. 6. Distribution of the CH_4 concentration for the four sampling campaigns. a) June 2008; b) March 2010; c) March 2011; and d) May 2012. Higher values are observed within the source zone limits, and lower concentrations are observed outside of the source zone.

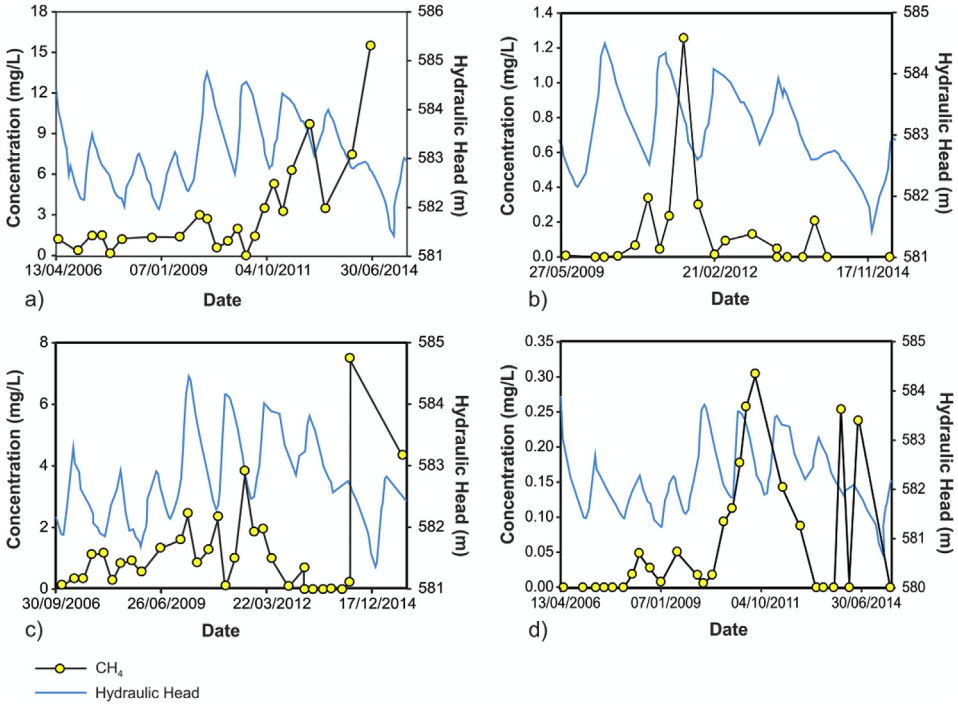

Fig. 7. Comparison of water table fluctuation and methane concentration variation over time. The sample locations are as follows: a) Well 32, center of the source zone; b) Well 81, downstream of the source zone; c) Well 67, downstream of the source zone; d) Well 30, downstream of the source zone.

bond.

$$CH_{4(aq)} + 2O_2 \rightarrow 2H_2O + CO_{2(aq)} \quad (6)$$

Despite Reactions 6 and 7 being normally associated with an oxidative environment, these reactions may occur in the anoxic source zone when air entrapment occurs. The Fe^{2+} and CH_4 concentration trends over time revealed that both were highly variable and inversely correlated to the temporal trends of the water table fluctuation (Figs. 5 and 7). The decrease in the by-product concentrations may be related to an increase in the oxidative reaction rates driven by the seasonal input of groundwater recharge. The air, which is entrapped during upward movement of the water table, promotes aquifer oxygenation and increases the by-product oxidation rates. Alternatively, during a recession period, groundwater is drained from the pore space, and most of the quasi-saturated zone disappeared, thereby critically reducing oxygen delivery to the saturated zone and reducing the by-product oxidation rates.

4.2.4. Effect of high PCO_2

Shallow groundwater is an open system buffered with high PCO_2 that is found in the unsaturated zone. Typical values of PCO_2 are estimated to fall within 10–1.8 to 10–1.4 atm in tropical regions (Brook et al., 1983). Bordignon et al. (2015) has revealed that the concentration of CO_2 that is in equilibrium with groundwater is high, reaching concentrations of over 45.000 ppmv. Another important finding from Bordignon et al. (2015) was that the amount of CO_2 produced by BTEX biodegradation and CH_4 oxidation was much smaller than the natural concentration of CO_2, since CO_2 concentrations in both the contaminated and uncontaminated portions of the aquifer were similar.

The speciation calculation of the pristine groundwater buffered by a PCO_2 level of $10^{-1.5}$ atm indicates a pH value of approximately 4.7 and an alkalinity value of less than 1 mg/L, which are similar to the field measurements. The pH values within the source zone are nearly 6, and the values gradually decline downgradient. The biodegradation under Fe(III) reduction explains the strong pH increase in the source zone, since the pH is related to the HCO_3^- concentration. Despite the strong correlation between the Fe^{2+} and HCO_3^- values observed in the field analysis (Fig. 7), the stoichiometric ratio of these species (2:1) does not follow that of Eq. (3) (7:36). However, in the presence of aqueous CO_2, 65 additional moles of HCO_3^- are added to the 7 that are derived from toluene oxidation, producing 72 mol of HCO_3^-, as shown in Eq. (7), which defines the proposed overall reaction of toluene mineralization via iron-reduction, incorporating the effect of PCO_2.

$$C_7H_8 + 36FeOOH + 14H_2O + 65CO_2 \rightarrow 72HCO_3^- + 36Fe^{2+} \quad (7)$$

Per Eq. (7), in the shallow unconfined aquifers where the carbonates are lacking, BTEX biodegradation under goethite reduction produces 2 mol of HCO_3^- for each mole of Fe^{2+}. Fig. 8 illustrates the scatterplot graph of the aqueous concentration of Fe^{2+} and alkalinity. Because the overall majority of the measured pH in the field falls within 4–6.5, the total alkalinity was assumed as the HCO_3^- concentration based on the equilibrium state. Since the stoichiometric ratio of Eq. (7) adjusts better to the observed field data than the stoichiometry of Eq. (2), Eq. (7) is most appropriate for describing the geochemical changes that are associated with BTEX mineralization.

The stoichiometry of Reaction 7 reveals that nearly 89% of the HCO_3^- (65 out of 72) that was produced by biodegradation under iron reduction was generated by the abiotic reaction with aqueous CO_2. Since high concentrations of Fe^{2+} and HCO_3^- were produced by hydrocarbon mineralization under Fe(III) reduction, as defined by the stoichiometric ratio of Eq. (7), the siderite saturation index was a useful indicator of this metabolic pathway in lateritic aquifers. Fig. 9 illustrates the distribution of the saturation index of siderite ($FeCO_3$), which confirms that samples collected inside of the LNAPL source zone are closer to saturation with respect to siderite than samples further downgradient. The reduction of siderite saturation is related to the decrease in both HCO_3^- and Fe^{2+} concentrations due to the reoxidation of Fe^{2+} and the precipitation of amorphous iron hydroxide downgradient of the source zone.

4.2.5. Geochemical zoning

From the available field data, a conceptual model is proposed based on the set of reactions that describe the geochemical changes observed in the field. In the proposed conceptual model, four reactions (Eqs. (1)–(7)) explain most geochemical changes in the aquifer. Due to BTEX biodegradation under Fe(III)-reduction coupled with methanogenesis, a reducing environment is observed with high Fe^{2+} and CH_4 concentrations within the source zone. Both Fe^{2+} and CH_4 are oxidized by a microbial-mediated reaction along the flow path, resulting in a decrease in concentration of these species. The Fe^{2+} oxidation also reduces the alkalinity and pH, resulting in the decrease in $SI_{Siderite}$. The redox condition and plume size are governed by the kinetics of the reactions involved.

The proposed conceptual model compartmentalizes the study area into the following four different redox zones (Fig. 10): (i) the background, (ii) the source zone, (iii) the BTEX plume and (iv) the by-products plume. Table 1 summarizes the average values of the physical-chemical parameters, BTEX, and the Fe^{2+} and CH_4 concentrations in each of the proposed geochemical zones.

5. Discussion

Based on the abovementioned statements, to guide the correct interpretation of the measured field data, a conceptual model covering the chemical equilibrium and the reactions related to hydrocarbon biodegradation in iron-rich aquifers in tropical environments was developed. Most likely, the redox values of the source zone (Table S1, Supplementary Material) and the Fe^{2+} and CH_4 concentrations would be too low if the oxygen were not released from the entrapped air. The calculation of biodegraded BTEX mass based solely on the stoichiometric conversion of the mass of both Fe^{2+} and CH_4 (Eqs. (2) and (3)) within the source zone may not provide accurate results since these species are subject to oxidation. Due to the wide range (> 2.0 m) of the water table fluctuation in the study site, there are favorable conditions for air entrapment. The entrapped air in the pores constitutes a medium-term source of oxygen (Haberer et al., 2014), raising the redox conditions of the contaminated groundwater.

The oxidation is related to oxygen availability driven by air entrapment and probably generates a seasonal variation in both Fe^{2+} and CH_4. Moreover, the water table fluctuation also governs the BTEX mineralization kinetics under iron reduction and methanogenesis. Consequently, a strong variation of Fe^{2+} and CH_4 is expected. The Fe^{2+} (Fig. 5) and CH_4 (Fig. 7) concentrations over time show high variability, with alternating cycles of increase and decrease concentrations displaying an inverse trend with respect to the water table fluctuation. Most likely, this variation may be linked to changes of redox state of the aquifer due to the influx of oxygen during water table rise (wet season) and consequent air entrapment in the uppermost portion of saturated zone. When water table falls (dry season) entrapped air is released, resulting in a more reduced environment.

Iron cycling within the source zone is a major issue in the bacterial assimilation of hydrocarbon, since both dissolution and precipitation of iron oxides may occur, changing the mineralogical composition of the aquifer. The oxygen quickly oxidizes the Fe^{2+} that initially precipitates as ferrihydrite, which is further converted to goethite. Most likely, in the absence of Fe^{2+} oxidation, the sediment would be depleted more intensely.

The microcosm experiments reproducing BTEX mineralization by iron reducer strains are always conducted under anoxic and closed environments (Lovley and Anderson, 2000; Baedecker et al., 1993; Botton and Parsons, 2007; Dorer et al., 2016). Thus, some important natural field constraints, such as PCO_2 and O_2 released from the

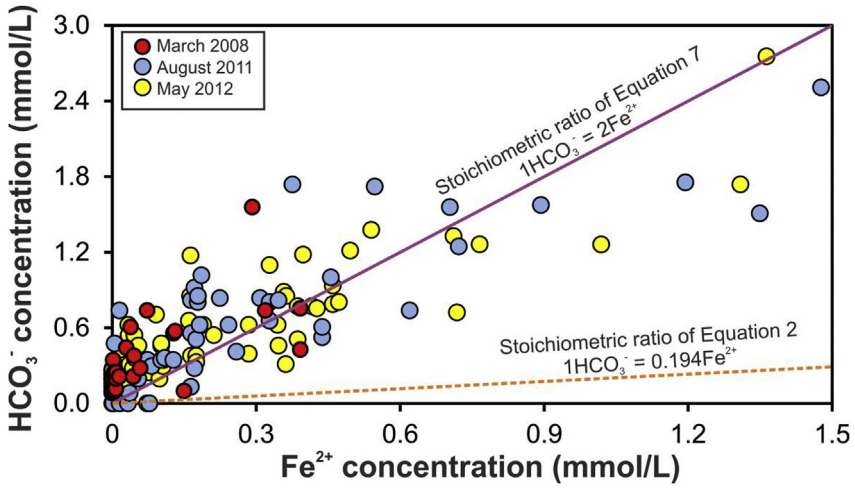

Fig. 8. Scatterplot of aqueous Fe^{2+} and total alkalinity values of the 3 sampling campaigns. The graph also illustrates the line of the stoichiometric ratio of Reactions 2 and 7. The trend line of Eq. (7) adjusts better to the field data than the trend line of Eq. (2).

entrapped air, are not reproduced. Because of this limitation, the biogeochemistry characterization of the microcosm experiments should not be directly used to guide the reactive transport simulation of the contaminated sites.

The high concentrations of both Fe(II) and CH_4 in the source zone (Figs. 4 and 6) indicate that iron reduction and methanogenesis occur simultaneously in BTEX mineralization. Higher CH_4 concentrations frequently occur when concentrations of Fe(II) are lower, suggesting a partial replacement of the metabolic pathway due to the iron depletion in some portions of the source zone. Since both pathways overlap in the source zone, the performed simulations were designed to reproduce the simultaneous biodegradation via both Fe(III) reduction and methanogenesis. To elucidate the overlap of iron reduction and methanogenesis, future investigations are needed to characterize the diversity and microbial community structures. Even though methanogenesis is traditionally recognized as a reaction with a low thermodynamic favorability, this reaction is an efficient pathway for contaminant mass destruction due to the syntrophic relationship (Morris et al., 2013; Gieg et al., 2014; Lueders and Muyzer, 2017).

The conceptual model that was developed in this work can satisfactorily explain the conditions observed in the field and may be applied to aquifers with similar characteristics, supporting the understanding of the natural attenuation processes and their effectiveness in limiting the spread of BTEX-dissolved phase plumes.

6. Conclusions

This work demonstrates the importance of the geochemical constraints related to BTEX biodegradation in tropical and subtropical aquifers, particularly for the naturally high PCO_2 levels and the by-product oxidation due to aquifer oxygenation by entrapped air. The proposed conceptual model is capable of explaining the field geochemistry, where the tropical and subtropical climate environments meet hydrological and geochemical conditions that affect the behavior of organic compounds in groundwater.

A significant amount of the reduced species (such as Fe^{2+} and CH_4) produced during BTEX biodegradation may be removed by microbial activity using the oxygen that diffuses from the entrapped air bubbles into the pore water. Therefore, since BTEX mass biodegradation may be measured by Fe^{2+} and CH_4 based on the stoichiometric ratio of Eqs. (4) and (5), the oxidation of these species underestimates the biodegradation rates.

The obtained results confirm that the observed field conditions cannot be explained without the equilibrium of high PCO_2 in an open system context. The PCO_2 buffer is the most important natural constraint for governing the carbonate saturations in the contaminated

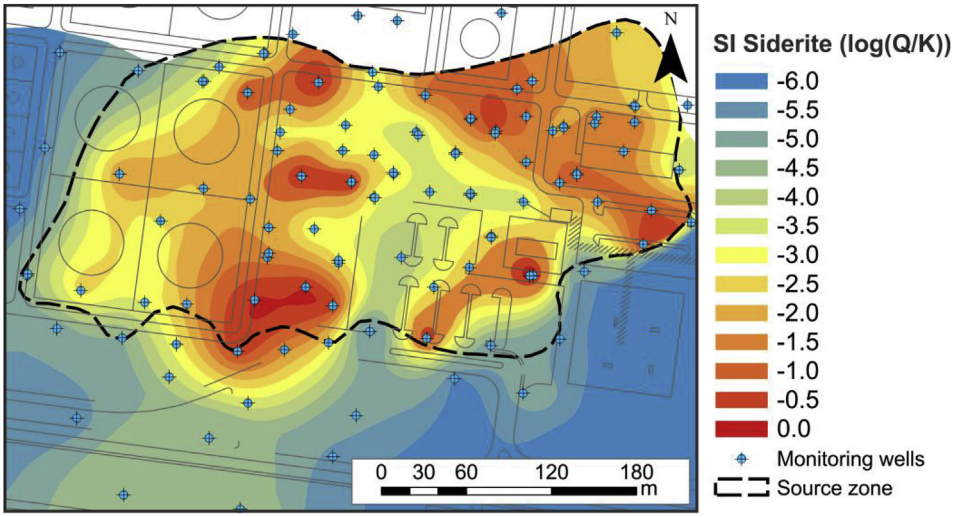

Fig. 9. Distribution of the siderite saturation index in the study area. The high SI values are observed in the source zone, and lower values are observed downgradient. The depleted central region is coincident with the zone of active Fe(III) reduction (see Fig. 4).

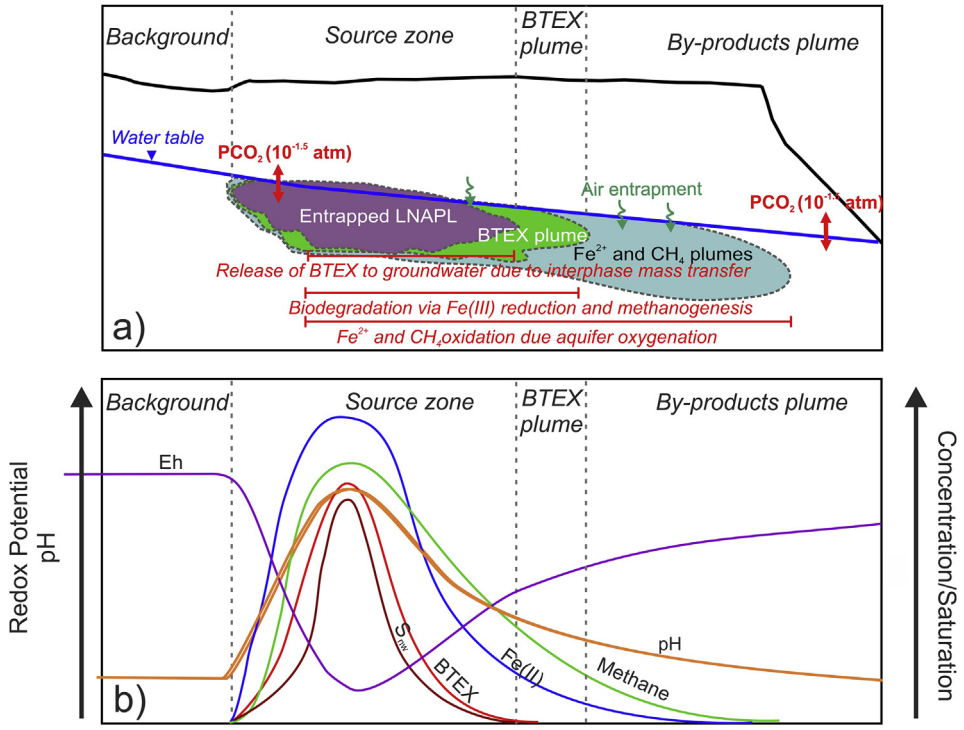

Fig. 10. a) Simplified cross-section of the conceptual model with the distribution of geochemical zones and the main reactions; b) concentration trend of BTEX and by-products along the flow path, LNAPL saturation (S_{nw}) within the source zone, pH and redox potential.

Table 1
Average values of the physical-chemical parameters of groundwater and the concentrations of BTEX and the by-products Fe^{2+} and CH_4 in each conceptualized zone (Fig. 10).

Geochemical Zone	BTEX (µg/l)	Fe^{2+} (mg/l)	CH_4 (mg/l)	Alkalinity (mg/l)	pH	EC (µS/cm)	Eh (mV)	SI Siderite Log (Q/K)
Background	0.000	0.023	0.002	6.33	4.71	11.37	281.50	< -6.00
By-products Plume	0.000	0.118	0.050	21.81	5.27	66.80	299.00	−5.38
BTEX Plume	22.26	12.052	1.94	39.17	5.47	89.36	130.80	−2.82
Source Zone	1777.82	16.401	2.543	44.05	5.62	101.33	−120.04	−1.82

lateritic aquifers.

Acknowledgments

We gratefully acknowledge Fundação para o Desenvolvimento da UNESP – FUNDUNESP, Laboratory of Basin Studies – LEBAC/UNESP and Petróleo Brasileiro S/A – PETROBRAS for their financial and technical support. We would like to thank the anonymous reviewers and the Associate Editor for their comments and suggestions, which have been very helpful in improving the manuscript.

Appendix A. Supplementary data

Supplementary data to this article can be found online at https://doi.org/10.1016/j.apgeochem.2018.11.019.

References

Amos, R.T., Mayer, K.U., 2006. Investigating the role of gas bubble formation and entrapment in contaminated aquifers: reactive transport modelling. J. Contam. Hydrol. 87 (1), 123–154. https://doi.org/10.1016/j.jconhyd.2006.04.008.

Appelo, C.A.J., Pstma, D., 2005. Geochemistry, Groundwater and Pollution, 2ª Edition. Balkema.

Baedecker, M.J., Cozzarelli, I.M., Eganhouse, R.P., Siegel, D.I., Bennett, P.C., 1993. Crude oil in a shallow sand and gravel aquifer—III. Biogeochemical reactions and mass balance modeling in anoxic groundwater. Appl. Geochem. 8 (6), 569–586. https://doi.org/10.1016/0883-2927(93)90014-8.

Baker, R.J., Baehr, A.L., Lahvis, M.A., 2000. Estimation of hydrocarbon biodegradation rates in gasoline-contaminated sediment from measured respiration rates. J. Contam. Hydrol. 41 (1), 175–192. https://doi.org/10.1016/S0169-7722(99)00063-7.

Beauvais, A., 1999. Geochemical balance of lateritization processes and climatic signatures in weathering profiles overlain by ferricretes in Central Africa. Geochem. Cosmochim. Acta 63 (23), 3939–3957. https://doi.org/10.1016/S0016-7037(99)00173-8.

Bekins, B.A., Cozzarelli, I.M., Godsy, E.M., Warren, E., Essaid, H.I., Tuccillo, M.E., 2001. Progression of natural attenuation processes at a crude oil spill site: II. Controls on spatial distribution of microbial populations. J. Contam. Hydrol. 53, 387–406. https://doi.org/10.1016/j.jconhyd.2009.12.001.

Borden, R.C., Gomez, C.A., Becker, M.T., 1995. Geochemical indicators of intrinsic bioremediation. Ground Water 33, 180–189. https://doi.org/10.1111/j.1745-6584.1995.tb00272.x.

Bordignon, R., Teramoto, E.H., Chang, K.H., 2015. Caracterização isotópica de CO_2 dissolvido em águas subterrâneas em área contaminada por querosene de aviação, município de Paulínia, SP. Águas Subterrâneas 29 (3), 301–314. https://doi.org/10.14295/ras.v29i3.27979.

Botton, S., Parsons, J.R., 2007. Degradation of BTX by dissimilatory iron-reducing cultures. Biodegradation 18 (3), 371–381. https://doi.org/10.1007/s10532-006-9071-9.

Breed, A.W., Dempers, C.J.N., Searby, G.E., Gardner, M.N., Rawlings, D.E., Hansford, G.S., 1999. The effect of temperature on the continuous ferrous-iron oxidation kinetics of a predominantly Leptospirillum ferrooxidans culture. Biotechnol. Bioeng. 65, 44–53.

Brook, G.A., Folkoff, M.E., Box, E.O., 1983. A world model of soil carbon dioxide. Earth Surf. Process. Landforms 8 (1), 79–88.

Chapelle, F.H., Lovley, D.R., 1992. Competitive exclusion of sulfate reduction by Fe (lll)-reducing bacteria: a mechanism for producing discrete zones of high-iron ground water. Ground Water 30 (1), 29–36. https://doi.org/10.1111/j.1745-6584.1992.tb00808.x.

Clark, I.D., Fritz, P., 1997. Environmental Isotopes in Hydrogeology. Lewis Publishers 331

págs.
Colombani, N., Mastrocicco, M., Gargini, A., Davis, G.B., Prommer, H., 2009. Modelling the fate of styrene in a mixed petroleum hydrocarbon plume. J. Contam. Hydrol. 105 (1), 38–55. https://doi.org/10.1016/j.jconhyd.2008.11.005.
Cozzarelli, I.M., Bekins, B.A., Baedecker, M.J., Aiken, G.R., Eganhouse, R.P., Tuccillo, M.E., 2001. Progression of natural attenuation processes at a crude-oil spill site: I. Geochemical evolution of the plume. J. Contam. Hydrol. 53 (3), 369–385. https://doi.org/10.1016/S0169-7722(01)00174-7.
Declercq, I., Cappuyns, V., Duclos, Y., 2012. Monitored natural attenuation (MNA) of contaminated soils: state of the art in Europe—a critical evaluation. Sci. Total Environ. 426, 393–405. https://doi.org/10.1016/j.scitotenv.2012.03.040.
Dixit, S., Hering, J.G., 2006. Sorption of Fe (II) and as (III) on goethite in single-and dual-sorbate systems. Chem. Geol. 228 (1), 6–15. https://doi.org/10.1016/j.chemgeo.2005.11.015.
Dorer, C., Vogt, C., Neu, T.R., Stryhanyuk, H., Richnow, H.H., 2016. Characterization of toluene and ethylbenzene biodegradation under nitrate-, iron (III)-and manganese (IV)-reducing conditions by compound-specific isotope analysis. Environ. Pollut. 211, 271–281. https://doi.org/10.1016/j.envpol.2015.12.029.
El Gheriany, I.A., Bocioaga, D., Hay, A.G., Ghiorse, W.C., Shuler, M.L., Lion, L.W., 2009. Iron requirement for Mn (II) oxidation by Leptothrix discophora SS-1. Appl. Environ. Microbiol. 75 (5), 1229–1235. https://doi.org/10.1128/AEM.02291-08.
Esther, J., Sukla, L.B., Pradhan, N., Panda, S., 2015. Fe (III) reduction strategies of dissimilatory iron reducing bacteria. Kor. J. Chem. Eng. 32 (1), 1–14. https://doi.org/10.1007/s11814-014-0286-x.
Faybishenko, B.A., 1995. Hydraulic behavior of quasi-saturated soils in the presence of entrapped air: laboratory experiments. Water Resour. Res. 31 (10), 2421–2435. https://doi.org/10.1029/95WR01654.
Fallgren, P.H., Jin, S., Zhang, R., Stahl, P.D., 2010. Empirical models estimating carbon dioxide accumulation in two petroleum hydrocarbon–contaminated soils. Ann. Finance 14 (2), 98–108. https://doi.org/10.1080/10889861003767084.
Fry, V.A., Selker, J.S., Gorelick, S.M., 1997. Experimental investigations for trapping oxygen gas in saturated porous media for in situ bioremediation. Water Resour. Res. 33 (12), 2687–2696. https://doi.org/10.1029/97WR02428.
Geistlinger, H., Beckmann, A., Lazik, D., 2005. Mass transfer between a multicomponent trapped gas phase and a mobile water phase: experiment and theory. Water Resour. Res. 41 (11). https://doi.org/10.1029/2004WR003885.
Geroni, J.N., Sapsford, D.J., 2011. Kinetics of iron (II) oxidation determined in the field. Appl. Geochem. 26 (8), 1452–1457. https://doi.org/10.1016/j.apgeochem.2011.05.018.
Gieg, L.M., Fowler, S.J., Berdugo-Clavijo, C., 2014. Syntrophic biodegradation of hydrocarbon contaminants. Curr. Opin. Biotechnol. 27, 21–29. https://doi.org/10.1016/j.copbio.2013.09.002.
Haberer, C.M., Rolle, M., Cirpka, O.A., Grathwohl, P., 2012. Oxygen transfer in a fluctuating capillary fringe. Vadose Zone J. 11 (3). https://doi.org/10.2136/vzj2011.0056.
Haberer, C.M., Cirpka, O.A., Rolle, M., Grathwohl, P., 2014. Experimental sensitivity analysis of oxygen transfer in the capillary fringe. Groundwater 52 (1), 37–49. https://doi.org/10.1111/gwat.12028.
Haberer, C.M., Rolle, M., Cirpka, O.A., Grathwohl, P., 2015a. Impact of heterogeneity on oxygen transfer in a fluctuating capillary fringe. Ground Water 53 (1), 57–70. https://doi.org/10.1111/gwat.121495.
Haberer, C.M., Muniruzzaman, M., Grathwohl, P., Rolle, M., 2015b. Diffusive-dispersive and reactive fronts in porous media: iron(II) oxidation at the unsaturated-saturated interface. Vadose Zone J. 14 (5). https://doi.org/10.2136/vzj2014.07.0091.
Hallbeck, L., Ståhl, F., Pedersen, K., 1993. Phytogeny and phenotypic characterization of the stalk-forming and iron-oxidizing bacterium Gallionella ferruginea. Microbiology 139 (7), 1531–1535. https://doi.org/10.1099/00221287-139-7-1531.
Heron, G., Crouzet, C., Bourg, A.C., Christensen, T.H., 1994. Speciation of Fe (II) and Fe (III) in contaminated aquifer sediments using chemical extraction techniques. Environ. Sci. Technol. 28 (9), 1698–1705. https://doi.org/10.1021/es00058a023.
Hinchee, R.E., Ong, S.K., 1992. A rapid in situ respiration test for measuring aerobic biodegradation rates of hydrocarbons in soil. J. Air Waste Manag. Assoc. 42 (10), 1305–1312. https://doi.org/10.1080/10473289.1992.10467077.
Holocher, J., Peeters, F., Aeschbach-Hertig, W., Kinzelbach, W., Kipfer, R., 2003. Kinetic model of gas bubble dissolution in groundwater and its implications for the dissolved gas composition. Environ. Sci. Technol. 37 (7), 1337–1343. https://doi.org/10.1021/es025712z.
Hunter, K.S., Wang, Y., Van Cappellen, P., 1998. Kinetic modeling of microbially-driven redox chemistry of subsurface environments: coupling transport, microbial metabolism and geochemistry. J. Hydrol. 209 (1), 53–80. https://doi.org/10.1016/S0022-1694(98)00157-7.
Katsoyiannis, I.A., Zouboulis, A.I., 2004. Biological treatment of Mn (II) and Fe (II) containing groundwater: kinetic considerations and product characterization. Water Res. 38 (7), 1922–1932. https://doi.org/10.1016/j.watres.2004.01.014.
Kessler, T.J., Harvey, C.F., 2001. Global flux of carbon dioxide into groundwater. Geophys. Res. Lett. 28 (2), 279–282. https://doi.org/10.1029/2000GL011505.
Klueglein, N., Lösekann-Behrens, T., Obst, M., Behrens, S., Appel, E., Kappler, A., 2013. Magnetite formation by the novel Fe (III)-reducing Geothrix fermentans strain HradG1 isolated from a hydrocarbon-contaminated sediment with increased magnetic susceptibility. Geomicrobiol. J. 30 (10), 863–873. https://doi.org/10.1080/01490451.2013.790922.
Lee, R.W., 1997. Effects of carbon dioxide variations in the unsaturated zone on water chemistry in a glacial-outwash aquifer. Appl. Geochem. 12 (4), 347–366. https://doi.org/10.1016/S0883-2927(97)00001-2.
Lovley, D.R., Anderson, R.T., 2000. Influence of dissimilatory metal reduction on fate of organic and metal contaminants in the subsurface. Hydrogeol. J. 8 (1), 77–88. https://doi.org/10.1007/PL00010974.
Lovley, D.R., Baedecker, M.J., Lonergan, D.J., Cozzarelli, I.M., Phillips, E.J., Siegel, D.I., 1989. Oxidation of aromatic contaminants coupled to microbial iron reduction. Nature 339 (6222), 297–300. https://doi.org/10.1038/339297a0.
Lueders, T., Muyzer, G., 2017. The ecology of anaerobic degraders of BTEX hydrocarbons in aquifers. FEMS Microbiol. Ecol. 93 (1). https://doi.org/10.1093/femsec/fiw220.
Macpherson, G.L., 2009. CO_2 distribution in groundwater and the impact of groundwater extraction on the global C cycle. Chem. Geol. 264 (1), 328–336. https://doi.org/10.1016/j.chemgeo.2009.03.018. 2009.
Marinas, M., Roy, J.W., Smith, J.E., 2013. Changes in entrapped gas content and hydraulic conductivity with pressure. Ground Water 51 (1), 41–50. https://doi.org/10.1111/j.1745-6584.2012.00915.x.
Martin, S.T., 2005. Precipitation and dissolution of iron and manganese oxides. In: Grassian, V.H. (Ed.), Environmental Catalysis. CRC Press, Boca Raton, FL, pp. 61–81.
Mayer, K.U., Frind, E.O., Blowes, D.W., 2002. Multicomponent reactive transport modeling in variably saturated porous media using a generalized formulation for kinetically controlled reactions. Water Resour. Res. 38 (9). https://doi.org/10.1029/2001WR000862.
McDonald, I.R., Miguez, C.B., Rogge, G., Bourque, D., Wendlandt, K.D., Groleau, D., Murrell, J.C., 2006. Diversity of soluble methane monooxygenase-containing methanotrophs isolated from polluted environments. FEMS Microbiol. Lett. 255 (2), 225–232. https://doi.org/10.1111/j.1574-6968.2005.00090.x.
McLeod, H.C., Roy, J.W., Smith, J.E., 2015. Patterns of entrapped air dissolution in a two-dimensional pilot-scale synthetic aquifer. Groundwater 53, 271–281. https://doi.org/10.1111/gwat.12203.
Miles, B., Peter, A., Teutsch, G., 2008. Multicomponent simulations of contrasting redox environments at an LNAPL site. Ground Water 46 (5), 727–742. https://doi.org/10.1111/j.1745-6584.2008.00457.x.
Miller, C.T., Poirier-McNeill, M.M., Mayer, A.S., 1990. Dissolution of trapped nonaqueous phase liquids: mass transfer characteristics. Water Resour. Res. 26 (11), 2783–2796. https://doi.org/10.1029/WR026i011p02783.
Morgan, B., Lahav, O., 2007. The effect of pH on the kinetics of spontaneous Fe (II) oxidation by O_2 in aqueous solution–basic principles and a simple heuristic description. Chemosphere 68 (11), 2080–2084. https://doi.org/10.1016/j.chemosphere.2007.02.015.
Morris, B.E., Henneberger, R., Huber, H., Moissl-Eichinger, C., 2013. Microbial syntrophy: interaction for the common good. FEMS (Fed. Eur. Microbiol. Soc.) Microbiol. Rev. 37 (3), 384–406. https://doi.org/10.1111/1574-6976.12019.
Mortazavi, B., Horel, A., Beazley, M.J., Sobecky, P.A., 2013. Intrinsic rates of petroleum hydrocarbon biodegradation in Gulf of Mexico intertidal sandy sediments and its enhancement by organic substrates. J. Hazard Mater. 244, 537–544. https://doi.org/10.1016/j.jhazmat.2012.10.038.
National Research Council, 2000. Natural Attenuation for Groundwater Remediation. National Academy Press, Washington, D.C, pp. 292.
Newby, D.T., Reed, D.W., Petzke, L.M., Igoe, A.L., Delwiche, M.E., Roberto, F.F., Colwell, F.S., 2004. Diversity of methanotroph communities in a basalt aquifer. FEMS Microbiol. Ecol. 48 (3), 333–344. https://doi.org/10.1016/j.femsec.2004.02.001.
Ng, G.H.C., Bekins, B.A., Cozzarelli, I.M., Baedecker, M.J., Bennett, P.C., Amos, R.T., 2014. A mass balance approach to investigating geochemical controls on secondary water quality impacts at a crude oil spill site near Bemidji, MN. J. Contam. Hydrol. 164, 1–15. https://doi.org/10.1016/j.jconhyd.2014.04.006.
Pede, M.A.Z., 2009. Flutuação do lençol freático e sua implicação na recuperação de hidrocarbonetos: um estudo de caso (Tese de Doutorado em Geociências e Meio Ambiente). .
Prommer, H., Barry, D.A., Davis, G.B., 2002. Modelling of physical and reactive processes during biodegradation of a hydrocarbon plume under transient groundwater flow conditions. J. Contam. Hydrol. 59 (1), 113–131. https://doi.org/10.1016/S0169-7722(02)00078-5.
Reguera, G., McCarthy, K.D., Mehta, T., Nicoll, J.S., Tuominen, M.T., Lovley, D.R., 2005. Extracellular electron transfer via microbial nanowires. Nature 435 (7045), 1098–1101. https://doi.org/10.1038/nature03661.
Rooney-Varga, J.N., Anderson, R.T., Fraga, J.L., Ringelberg, D., Lovley, D.R., 1999. Microbial communities associated with anaerobic benzene degradation in a petroleum-contaminated aquifer. Appl. Environ. Microbiol. 65 (7), 3056–3063.
Schreiber, M.E., Carey, G.R., Feinstein, D.T., Bahr, J.M., 2004. Mechanisms of electron acceptor utilization: implications for simulating anaerobic biodegradation. J. Contam. Hydrol. 73 (1), 99–127. https://doi.org/10.1016/j.jconhyd.2004.01.004.
Schwertmann, U., 1988. Occurrence and formation of iron oxides in various pedoenvironments. In: Iron in Soils and Clay Minerals. Springer Netherlands, pp. 267–308.
Shirokova, V.L., Enright, A.M.L., Kennedy, C.B., Ferris, F.G., 2016. Thermal intensification of microbial Fe (II)/Fe (III) redox cycling in a pristine shallow sand aquifer on the Canadian Shield. Water Res. 106, 604–612. https://doi.org/10.1016/j.watres.2016.10.050.
Sihota, N.J., Mayer, K.U., 2012. Characterizing vadose zone hydrocarbon biodegradation using carbon dioxide effluxes, isotopes, and reactive transport modeling. Vadose Zone J. 11 (4). https://doi.org/10.2136/vzj2011.0204.
Tardy, Y., Nahon, D., 1985. Geochemistry of laterites, stability of Al-goethite, Al-hematite, and Fe3 + -kaolinite in bauxites and ferricretes: an approach to the mechanism of concretion formation. Am. J. Sci. 285 (10), 865. https://doi.org/10.2475/ajs.285.10.865.
Teramoto, E.H., Chang, H.K., 2017. Field data and numerical simulation of btex concentration trends under water table fluctuations: example of a jet fuel-contaminated site in Brazil. J. Contam. Hydrol. 198, 37–47.
Vencelides, Z., Sracek, O., Prommer, H., 2007. Modelling of iron cycling and its impact on the electron balance at a petroleum hydrocarbon contaminated site in Hnevice, Czech Republic. J. Contam. Hydrol. 89 (3), 270–294. https://doi.org/10.1016/j.jconhyd.

2006.09.003.
Vollrath, S., Behrends, T., Koch, C.B., Van Cappellen, P., 2013. Effects of temperature on rates and mineral products of microbial Fe (II) oxidation by Leptothrix cholodnii at microaerobic conditions. Geochem. Cosmochim. Acta 108, 107–124. https://doi.org/10.1016/j.gca.2013.01.019.
Weber, K.A., Achenbach, L.A., Coates, J.D., 2006. Microorganisms pumping iron: anaerobic microbial iron oxidation and reduction. Nat. Rev. Microbiol. 4 (10), 752–764. https://doi.org/10.1038/nrmicro1490.
Wiedemeier, T.H., Rifai, H.S., Newell, C.J., Wilson, J.T., 1999. Natural Attenuation of Fuels and Chlorinated Solvents in the. Subsurface Wiley, New York, NY.
Williams, M.D., Oostrom, M., 2000. Oxygenation of anoxic water in a fluctuating water table system: an experimental and numerical study. J. Hydrol. 230 (1), 70–85. https://doi.org/10.1016/S0022-1694(00)00172-4.
Yurt, N., Sears, J., Lewandowski, Z., 2002. Multiple substrate growth kinetics of Leptothrix discophoraSP-6. Biotechnol. Prog. 18 (5), 994–1002. https://doi.org/10.1021/bp0255098.